

# Cryogenic System Preliminary Design for a 0.5m-long, Conduction-cooled Nb<sub>3</sub>Sn Undulator Magnet Prototype

Danlu Zhang, Ibrahim Kesgin, Yuko Shiroyanagi, Joel Fuerst, Yury Ivanyushenkov

**Abstract**— There are several NbTi superconducting undulator (SCU) magnets currently in operation at the Advanced Photon Source (APS) at Argonne National Laboratory (ANL). The development on Nb<sub>3</sub>Sn-based superconducting undulator magnets at APS is underway due to the potential to further enhance the performance of the SCUs. Superconducting undulator magnets need to keep temperature gradients minimized in order to retain thermal and operating current margin. We have designed the thermal links for efficient heat conduction using 3D finite element analysis (FEA) simulation in COMSOL Multiphysics software, which was later used for the calculation of the temperature distribution across a 0.5 m long, conduction-cooled, Nb<sub>3</sub>Sn undulator magnet prototype that includes both conductive heat transfer and radiative heating components. We have modelled the evolution of the thermal properties of the magnet winding as well as other cold parts during cool-down from ambient temperature with the operation of a SHI RDK-415D cryocooler to examine the estimated time that is needed for the cooldown as well as the baseline temperature we could achieve. A key result was that a maximum coil  $\Delta T = 0.11$  K along the designed thermal links and a temperature range of 3.42 K – 3.53 K for the winding were predicted at steady state. A pair of G10 support rods for carrying the magnet as well as a pair of current leads made of metals were also designed and optimized for the testing system, targeting for an operation temperature of 4 K and a coil current of 950 A DC.

**Index Terms**—Nb<sub>3</sub>Sn, superconducting magnets, FEA, thermal, current lead

## I. INTRODUCTION

Currently three superconducting undulators (SCUs) are installed and in operation at the Advanced Photon Source (APS) storage ring at Argonne National Laboratory. These NbTi superconducting magnets are cooled indirectly with LHe penetrating through channels from the helium tank attached to the system. However, conduction-cooling has been demonstrated as a reliable alternative to cool the superconducting magnets by a few groups [1-3]. As pointed out in reference [4] on the conceptual design of a conduction-cooled system for NbTi superconducting undulators at APS, a conduction-cooling system for undulators simplifies the cryostat design and its associated infrastructure. In addition, the use of conduction-cooling technology can alleviate the reliance on the highly-priced, non-renewable liquid Helium (LHe).

This work was supported by the U.S. Department of Energy, Office of Science, under Contract No. DE-AC02-06CH11357. (*Corresponding author: Danlu Zhang.*)

The authors are with the Advanced Photon Source, Argonne National Laboratory, Lemont, IL 60439 USA (e-mail: danlu.zhang@anl.gov).

Since NbTi SCU technology is close to its full potential, Nb<sub>3</sub>Sn has been identified as a promising candidate to further enhance the performance of undulators operated at the Advanced Photon Source (APS) [5] mainly due to the higher critical current density associated with Nb<sub>3</sub>Sn conductors at 4.2 K. A peak magnetic field of 1.2 T on the axis was seen for the Nb<sub>3</sub>Sn undulators designed for operation with 850 A at 4.2 K [6]. There are a number of experiments [5-7] have been successfully executed on a few short Nb<sub>3</sub>Sn undulator magnet prototypes at APS to date. These magnets are expected to be installed with an indirect LHe cooling channel for operation at 4.2 K with a designed current of 850 A to achieve an undulator peak field of 1.2 T. However, it is also desirable to study the conduction-cooling method for the cooling and operation of these undulator magnets due to the benefits mentioned in the previous paragraph.

A few conduction-cooled Nb<sub>3</sub>Sn magnets have been designed, tested and analyzed. Michael *et al.* [8] have used a 2-stage Gifford-McMahon (GM) cycle cryocoolers to test a 62 mm-tall, Nb<sub>3</sub>Sn prototype magnet for superconducting cyclotron. A total of 9 days were used to cool the magnet assembly below 4 K. Dhuley *et al.* [9] designed the thermal links carefully for the conduction-cooling of Nb<sub>3</sub>Sn SRF cavities by taking account of the measured thermal contact resistance of Al and Nb. Loder *et al.* [10] also described a detailed design of a 6-T, conduction-cooled, Nb<sub>3</sub>Sn superconducting racetrack coil with the help of ANSYS to get thermal gradient along the magnet as well as the strain generated on the winding at cryogenic temperatures with the various materials in the winding.

## II. THE SUPERCONDUCTING MAGNET SYSTEM

The superconducting magnet system is targeted for an operation at 4.2 K with a DC current of 950 A. The system is composed of the main components including the 0.5-m long Nb<sub>3</sub>Sn superconducting magnet prototype, the current leads, the cooling system and the mechanical supports for suspending the magnet and its associated instrumentation. This paper aims to use the finite element software, COMSOL, to draw the geometry of the 3D magnet prototype and then design the optimized metal conductor current leads for the current injection into the

Color versions of one or more of the figures in this paper are available online at <http://ieeexplore.ieee.org>.

Digital Object Identifier will be inserted here upon acceptance.

coil from room temperature to one end of the HTS leads thermally anchored at the 1<sup>st</sup> stage of the RDK-415D cryocooler. In addition, the supporting structure has also been designed for suspending the magnet for this system. In the end, the heat loads from various components in the magnet system have been identified and quantified to verify the simulation results. The physics used for the conduction cooldown in COMSOL is heat transfer coupled with surface-to surface radiation. The governing equations uses are:

$$\rho C_p \partial T / \partial t + \nabla \cdot (q + q_r) = Q \quad (1)$$

where  $\rho$  is the density [kg/m<sup>3</sup>],  $C_p$  is the specific heat capacity [J/(kg·K)], and  $T$  is temperature [K]. The heat flux  $q$ , is the conductive heat flux [W/m<sup>2</sup>] and  $q_r$  is the radiative heat flux [W/m<sup>2</sup>], respectively. The surface radiation flux [W/m<sup>2</sup>], which is applied to the outer surface of a solid domain in the model can be expressed as:

$$P_r [\text{W}] = A_i F_{ij} \sigma \varepsilon_i (T_i^4 - T_j^4) \quad (2)$$

where  $P_r$  is the surface radiative power [W] transferred from hot surface  $i$  to cold surface  $j$ .  $T_i$  is the temperature [K] of surface  $i$  and  $T_j$  is the surface temperature [K] of the surface  $j$ ,  $A_i$  is the surface area of body  $i$  [m<sup>2</sup>],  $F_{ij}$  is the view factor (the proportion of the radiation which leaves surface  $A$  that strikes surface  $B$ ),  $\sigma$  is the Stefan-Boltzmann constant [W/(m<sup>2</sup>K<sup>4</sup>)] and  $\varepsilon_i$  is the emissivity of surface  $i$ . The thermal conductivity values [11-15] and the specific heat values [12-13, 16-18] used in the model are temperature dependent.

### A. The Superconducting Magnet

The dimensions of the magnet and the design details of the superconducting undulator were mentioned in [6]. One 0.5 m-long Nb<sub>3</sub>Sn superconducting magnet prototype has 53 grooves and roughly used a conductor length of 589 m. Each winding groove has 46 turns of Nb<sub>3</sub>Sn RRP 144/169 conductor whose bare wire diameter is 0.6 mm. Each winding groove has a cross section dimension of about 5.5 mm wide by 4.9 mm high and the dimensions of the steel poles are about 4.8 mm high and 3.3 mm wide. Low carbon steel core (1006) was used for the strengthening of the magnetic field.

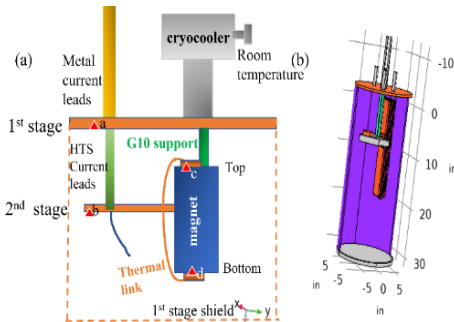


**Fig. 1.** (a) Schematic of the superconducting magnet prototype system (with one 2-stage cryocooler, unshown 2 G10 supports, the copper thermal link, metal current leads, as well as the magnet prototype). Triangles are where the temperature probes are attached in the simulation model; (b) The geometry of the magnet system including two stages of the cold head, metal current leads and the cold mass is made in COMSOL.

To see the feasibility of using a conduction-cooled cryostat to cool the 0.5 m-long, superconducting magnet prototype in a reasonable time, the targeted temperature of operation for this magnet with the conduction-cooling system is set to be around 4.2 K to match the performance that has been measured and confirmed previously in liquid helium cryogen [5,6].

### B. Optimization of Current Leads

In order to inject a DC current of 950 A into the magnet, current leads are designed to maximize the performance of the magnet system. High-temperature superconducting (HTS) current leads (using BSCCO conductors) were used and thermally anchored in between the 1<sup>st</sup> stage and the 2<sup>nd</sup> stage to conduct current. For the current transport portion from the room-temperature power supply to one end of the HTS leads anchored on the 1<sup>st</sup> stage, (27-cm long) metal current leads that made of both Cu (RRR = 60) and a specific copper alloy CuCrZr were considered as potential candidates.

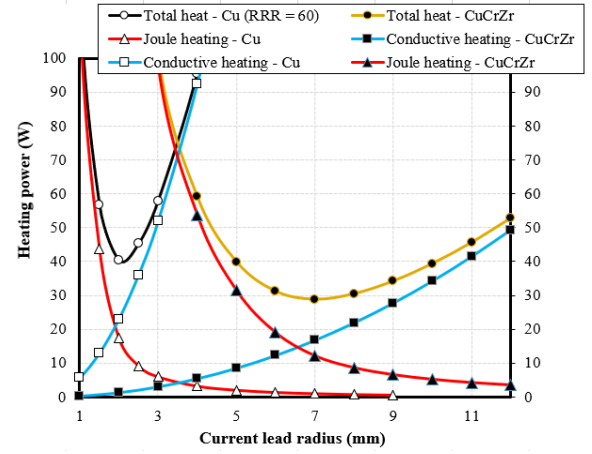


**Fig. 2.** Simulated heating power for current leads made with Cu and CuCrZr alloys is compared for various radii.

Care was taken to make sure the heat leak from both joule heating and conductive heating is minimized for the conduction of 950 A through the leads. For the finite element modeling of optimized current leads running from room temperature end to the end of the HTS leads on the 1<sup>st</sup> stage, joule heating due to current injection and conductive heat load due to temperature gradient along the current lead conductors were considered. The 300 K for the room temperature end and 50 K for the assumed 1<sup>st</sup> stage temperature where the leads are thermally anchored to. Results of the two heating power components associated with the current lead in the model were shown in Fig. 2. As expected, with the increase of the radius of the current lead in the model, the conduction heating power generated due to the temperature gradient alone increases. Meanwhile, the heating power for the joule heating component that is associated with the current lead decreases as the current lead cross section increases. Accordingly, we were able to find the minimal total heating power of about 28 W for a CuCrZr current lead with a radius of 7 mm. In addition, the minimal total heating power of about 40 W was

identified for the 4 mm-thick current lead made of pure Cu. This is not a surprise since the minimum energy transmitted from a high temperature ( $T_H$ ) to a low cold temperature  $T_L$  is given by McFee formulation:  $(\frac{k}{\sigma})_{avg} = \frac{1}{T_H - T_L} \int_{T_L}^{T_H} (\frac{k}{\sigma}) dT$  [19]. In this equation,  $T_H$  [K] represents the surface with high temperature,  $T_L$  [K] represents the surface with low temperature,  $k$  is the thermal conductivity [W/(mK)] of the current leads,  $\sigma$  [S/m] is the electrical conductivity of the current leads. The minimized thermal loading is for materials with the lowest ratio of thermal to electrical contributions. With this in mind, another 3D finite element model in COMSOL was built to incorporate the Cu-CrZr leads to enable a more precise analysis of the heat loads for the magnet system.

### C. The Cooling System

The Nb<sub>3</sub>Sn magnet prototype is thermally connected to the 2<sup>nd</sup> stage cold head of the RDK-415 D cryocooler through thermal links. In order to reach a low temperature gradient along the length of the magnet, both ends of the magnet are designed to be cooled by copper pieces that are secured at the ends of the magnet. These copper flat pieces then are connected to the copper thermal links that are anchored on the 2<sup>nd</sup> stage of the cold head. To maximize the contact area between the magnet and the 2<sup>nd</sup> stage cooling surface, the middle portion of the magnet is also designed to sit securely against the 2<sup>nd</sup> stage of the cold head. The 1<sup>st</sup> stage of the cold head is thermally connected to an 84 cm-long, cylinder-shaped radiation shield, where layers of MLI are attached to keep the cold mass shielded from the high thermal radiation from the surrounding high temperature (room temperature on the outside surfaces of the cryostat). The emissivity values of the radiative surfaces in the model have been included in TABLE I. The emissivity values were obtained from literature [20-21] and these could vary depending on the surface condition (roughness, oxidation etc).

Each stage of the GM cryocooler here has a changing cooling capacity based on the temperature of each stage. The map of cooling capacity as a function of temperature has been obtained for time-dependent cooldown modeling. The thermal links are designed here to minimize the thermal resistance based on equation  $R_\theta = \frac{\Delta x}{A \cdot k}$ , where  $R_\theta$  [K/W] refers to the absolute thermal resistance across the thickness of the thermal links,  $\Delta x$  is the thickness of the thermal link, and  $k$  is the temperature dependent thermal conductivity,  $A$  is the cross-sectional area that is perpendicular to the heat flow direction. It is also worth noticing that the thermal contact between the copper thermal link and the copper second stage has been set to be 20 W/(cm<sup>2</sup> K), assuming a ZnO grease will be applied in between these contacting surfaces. The same contact thermal conductance has been applied to the interfaces between the copper thermal link end and the copper flat pieces that are attached to the ends of the magnet.

### D. Mechanical Supports

G10 supports were chosen to be for suspension of the magnet on the 1<sup>st</sup> stage of the cryostat due to relatively low thermal conductivity and high tensile stress. To obtain the size of the rods for suspension, we first estimated the total mass of the magnet, the thermal link and the assembly associated with the instrumentation of the magnet, which was about 21 kg. Then we used a length of about 5 cm to connect the magnet from the 1<sup>st</sup> stage to the top of the magnet assembly. With the known tensile stress of G10 (2.76 E+8 Pa), we used 80% of this tensile stress as a safety criterion and calculated a “safe” radius of 5 mm (10% of the radius value based on the method mentioned here) for the G10 rods used for suspension.

## III. RESULTS OF THE THERMAL MODEL

### A. The Cooling Curves

The cooling curves for the 1<sup>st</sup> stage (probe *a* in Fig. 1) and 2<sup>nd</sup> stage (probe *b* in Fig. 1) are shown below in Fig. 3. As can be seen from the cooling curves, the 1<sup>st</sup> stage took about 18 hours to reach the baseline temperature for the second stage, whereas the 1<sup>st</sup> stage took about 50 hours to reach the baseline temperature. The baseline temperatures for the 1<sup>st</sup> stage and the 2<sup>nd</sup> stage are 55 K and 3.42 K, respectively.

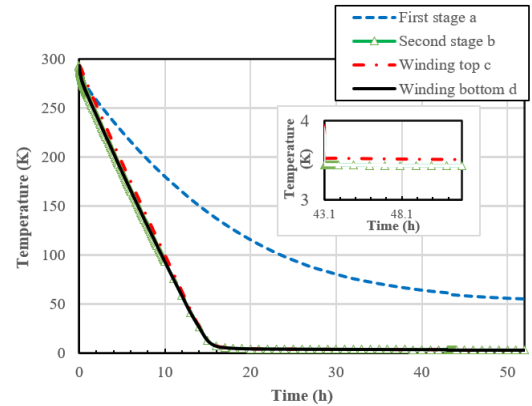


**Fig. 3.** Cooling curves as a function of time for temperature changes of four various temperature probes in Fig.1.

### B. Heat Load Breakdown

To verify the simulation and evaluate the detailed heat loads in the system, a breakdown of the steady state heat loads from various components on the 1<sup>st</sup> stage and 2<sup>nd</sup> stage is shown in TABLE 1. The dominant heat source on the 1<sup>st</sup> stage is conduction heat, this can be further reduced by selecting materials with even lower average  $(\frac{k}{\sigma})_{avg}$ . The heat load from the current leads is conduction heat only, since there is no injection of DC current during conduction-cooldown, only till the baseline temperature is reached, the current will be injected into the coil. Thus, the heat load from the leads is lower than the total heat calculated from Fig. 2. Meanwhile, the total heat loads on

different cooling stages in Table I were obtained from postprocessing the simulation result. With these total thermal powers as well as the cryocooler cooling curves given in Fig. 4, we were able to verify the temperature on the system by looking up the temperature associated with the certain cooling power in Fig. 4. In the end, the cooling power of the system equals the calculated heat loads when a steady state is reached.

**TABLE I**  
THE MAGNET SYSTEM  
HEAT LOAD BREAKDOWN AT THE STEADY STATE ON THE 2 STAGES

Heat Load	Power (W)
1 <sup>st</sup> stage	
Thermal radiation from top and middle MLI blankets (0.03)	16.027
Thermal radiation from bottom (0.07)	3.325
Conduction heat from metal current leads	32.759
<b>Total</b>	<b>52.11</b>
2 <sup>nd</sup> stage	
Thermal radiation from the 1 <sup>st</sup> stage	0.447
HTS current leads	0.039
2 G10 support rods	0.022
Instrumentation wires	0.020
<b>Total</b>	<b>0.53</b>

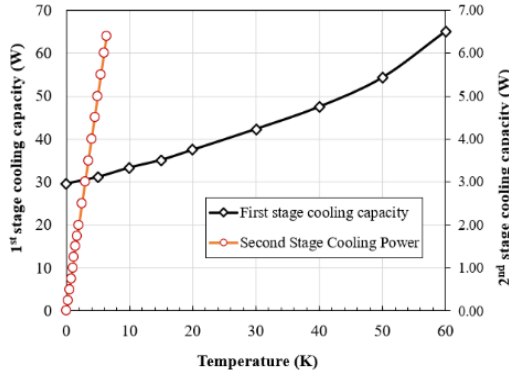


**Fig. 4.** Cooling power as a function of temperature for each stage of the cryocooler cold head (RDK-415D) used in the model.

The temperature distribution along the magnet and the thermal link have been shown in Fig. 5. It can be seen that the temperature along the magnet is 3.42 K – 3.53 K. The targeted temperature of 4.2 K can be realized from this conduction-cooling design, even though certain surface conditions (such as smooth surfaces of the metal to ensure low emissivity and well-sealed MLI blankets) have to be met for the experiment in reality.

#### IV. THERMAL CONTRACTION DURING COOLDOWN

Since the lowest temperature achieved in the cooldown model is around 4 K, a large temperature change during the cooldown process results in thermal shrinkage on different components in the magnet system due to the different thermal expansion coefficient values associated with different

materials. Literature has shown the thermal shrinkages of copper and steel are 3.25 mm and 2.25 mm per meter [22] when cooled from room temperature to 4 K. For our 0.5 m-long magnet, we would expect a shrinkage of 1.625 mm for copper and 1.125 mm for steels after conduction cooldown is stabilized. This 0.5 mm shrinkage has been considered in the copper thermal link designs in the model and the contact between the thermal links and the magnet should remain to be the same as when the cooling first gets started as long as the mechanical joint between the surfaces is secure.

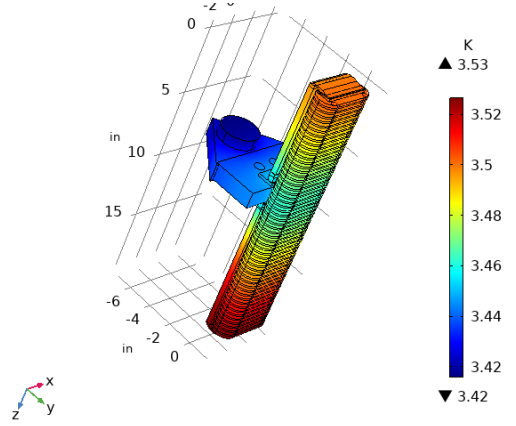


**Fig. 5.** Steady state temperature distribution along the superconducting magnet prototype. The copper thermal links and copper flat pieces at the ends of the magnet were connected to the 2<sup>nd</sup> stage of the cryocooler.

#### V. FUTURE WORK

The simulated work has provided promising results for the upcoming experimental work to validate the data obtained in this paper. In the future, the 0.5m-long, Nb<sub>3</sub>Sn undulator magnet prototype is expected to be cooled down using the designs of the mechanical support and the metal current leads from room temperature to the first stage. AC loss will also be considered in the thermal model in the future during the current charging of the magnet.

#### VI. CONCLUSIONS

Two FEM models have been built using COMSOL to study the cooldown time and baseline temperature of the magnet system that carries a conduction-cooled, 0.5 m long, Nb<sub>3</sub>Sn undulator magnet prototype. The baseline target temperature for the 0.5 m magnet was 3.42 – 3.53 K, meeting the design target of 4.2 K. And the baseline temperature for the 1<sup>st</sup> stage was 55 K. A breakdown of heat loads on 2 stages of the cold head has been shown with details. The metal current leads running from room temperature to one end of the HTS leads that is connected to the 1<sup>st</sup> stage are designed and optimized for the conduction-cooled Nb<sub>3</sub>Sn magnet prototype with a DC current of 950 A. A metal current lead made of CuCrZr alloys has shown a minimal heating power of 28 W with 950 A injection. The G10 supports for suspension of the magnet were also designed.

## REFERENCES

- [1] S. Casalbuoni, "A review of magnetic field measurements of full scale conduction cooled superconducting undulator coils," *Supercond. Sci. Technol.*, vol. 32, no. 2, p. 023001, Dec. 2018, Art. no. 023001.
- [2] C. Boffo, T. Gerhard, M. Turenne, W. Walter, S. Casalbuoni, A. Cecilia, S. Gerstl, A. Grau, T. Holubek, C. Meuter, DS. de Jauregui., "Performance of SCU15: The New Conduction-Cooled Superconducting Undulator for ANKA," *IEEE Trans. Appl. Supercond.*, vol. 26, no. 4, pp. 1–4, Jun. 2016, Art. no. 4102404.
- [3] D. Zhang, C. Kovacs, J. Rochester, M. Majoros, F. Wan, M.D. Sumption, E.W. Collings, M. Rindfleisch, D. Panik, D. Doll, R. Avonce et al., "Instrumentation, cooling, and initial testing of a large, conduction-cooled, react-and-wind MgB<sub>2</sub> coil segment for MRI applications," *Supercond. Sci. Technol.*, vol. 31, no. 8, p. 085013, Jul. 2018, Art. no. 085013.
- [4] Y. Shiroyanagi, Q. Hasse, M. Kasa, I. Kesgin, and Y. Ivanyushenkov, "Conceptual design of a conduction-cooled superconducting undulator," *IEEE Trans. Appl. Supercond.*, vol. 30, no. 4, pp. 1–4, Jun. 2020, Art. no. 4102004.
- [5] I. Kesgin, M. Kasa, S. MacDonald, Y. Ivanyushenkov, Y. Shiroyanagi, Q. Hasse, E. Barzi, D. Turrioni, A.V. Zlobin, E. Gluskin, "Fabrication and Testing of 10-Pole Short-Period Nb<sub>3</sub>Sn Superconducting Undulator Magnets," *IEEE Trans. Appl. Supercond.*, vol. 30, no. 4, pp. 1–5, Jun. 2020, Art. no. 4100605.
- [6] I. Kesgin, M. Kasa, S. MacDonald, Y. Ivanyushenkov, E. Barzi et al., "Fabrication and Testing of 18-mm-Period, 0.5-m-Long Nb<sub>3</sub>Sn Superconducting Undulator," *IEEE Trans. Appl. Supercond.*, vol. 31, no. 5, pp. 1–5, Aug. 2021, Art. no. 3057846.
- [7] I. Kesgin, M. Kasa, S. MacDonald, D. Turrioni, E. Barzi, Y. Shiroyanagi, Q. Hasse, Y. Ivanyushenkov, A. V. Zlobin, E. Gluskin, "Design, Construction, and Testing of 0.5-m, 18-mm Period Nb<sub>3</sub>Sn Superconducting Undulator Magnets," *IEEE Trans. Appl. Supercond.*, vol. 32, no. 6, pp. 1-5, Feb. 2022, Art. no. 4100605.
- [8] P. C. Michael, T. A. Antaya, A. Radovinsky, B. A. Smith, S. Pourrahimi, "Test of a conduction-cooled, prototype, superconducting magnet for a compact cyclotron," *IEEE Trans. Appl. Supercond.*, vol. 23, no. 3, Dec. 2012, Art. no. 4100304.
- [9] R. C. Dhuley, R. Kostin, O. Prokofiev, M. I. Geelhoed, T. H. Nicol, S. Posen, J. C. Thangaraj, T. K. Kroc, R. D. Kephart, "Thermal link design for conduction cooling of SRF cavities using cryocoolers," *IEEE Trans. Appl. Supercond.*, vol. 29, no. 5, pp.1-5, Feb. 2019, Art. no. 0500205.
- [10] D. Loder, R. Sanchez, M. Feddersen, K. Haran, M. Sumption, M. Tomsic, J. Yue, and D. Doll, "A conduction cooled Nb<sub>3</sub>Sn racetrack coil: Design, construction, and testing," 2016 IEEE Power and Energy Conference at Illinois (PECI), Feb. 2016, doi: 10.1109/peci.2016.7459230.
- [11] G. Manfreda, "Review of ROXIE's material properties database for quench simulation," TE Technology department internal note, Dec. 2011, 35.
- [12] K. S. Shibib, M. A. Minshid, M. M. Tahir, "Finite element analysis of spot laser of steel welding temperature history," *Therm. Sci.*, vol. 13, no. 4, pp. 143-50, 2019.
- [13] A. A. Amin, L. Sabri, C. Poole, T. Baig, R. J. Deissler, M. Rindfleisch, D. Doll, M. Tomsic, O. Akkus, M. Martens, "Computational homogenization of the elastic and thermal properties of superconducting composite MgB<sub>2</sub> wire," *Compos. Struct.* pp. 313-329, Mar. 2018
- [14] A. K. Dhami, M. K. Chattopadhyay, T. K. Dey, "Thermal Conductivity of 2223 BSCCO Superconductor–Polyethylene Glycol Composites Between 20 and 300 K," *J. Supercond.*, pp. 417-22, Jun. 2000.
- [15] J. S. Zhang, Y. T. Song, W. Q. Zhang, F. Jiang, "Magnetic and Thermal Design of HTS Quadrupole Magnet for Newly Developed Superconducting Proton Cyclotron Beam Line," *J. Supercond. Nov. Magn.*, pp. 529-38, vol. 32, no. 3, Mar. 2019.
- [16] K. Shinozaki, T. Mizutani, T. Fujii, T. Onaka, T. Nakagawa, H. Sugita, "Thermal property measurements of critical materials for SPICA payload module," *Phys. Procedia.*, vol. 67, pp. 270-5, Jan. 2015.
- [17] J. O. Odhiambo, and J. W. Makokha, "Specific heat and entropy of a three-electron model in bismuth based cuprate superconductor." (2018).
- [18] C.S. Myers, M.A. Susner, L. Motowildo, J. Distin, M.D. Sumption and E.W. Collings, "Specific Heats of Composite Bi2212, Nb<sub>3</sub>Sn and MgB<sub>2</sub> Wire Conductors", *IEEE Trans. Appl. Supercond.*, vol. 23, no. 3, p. 8800204, Jun. 2013.
- [19] L. Bromberg, P. C. Michael, J. V. Minervini, C. Miles, and J. G. Weisend, "Current lead optimization for cryogenic operation at intermediate temperatures," AIP Conference Proceedings, 2010, doi: 10.1063/1.3422405.
- [20] B. Window, G. Harding, "Thermal emissivity of copper," *JOSA.* vol. 71, no.3, pp. 354-357.
- [21] T. Miyakita, R. Hatakenaka, H. Sugita, M. Saitoh, T. Hirai, "Development of a new multi-layer insulation blanket with non-interlayer-contact spacer for space cryogenic mission," *Cryogenics*, vol. 64, pp.112-120.
- [22] J. Ekin, *Experimental Techniques for Low-Temperature Measurements*. Oxford University Press, 2006.